analytical chemistry

Article

pubs.acs.org/ac

Multidimensional Analysis of 16 Glucose Isomers by Ion Mobility Spectrometry

M. M. Gaye,* G. Nagy, D. E. Clemmer, and N. L. B. Pohl

Department of Chemistry, Indiana University, Bloomington, Indiana 47405, United States

Supporting Information

ABSTRACT: Diastereomeric adducts comprising an enantiomerically pure monosaccharide analyte, a peptide, and/or an amino acid and a divalent metal ion (for 16 different monosaccharide isomers) are generated by electrospray ionization and analyzed by combined ion mobility spectrometry-mass spectrometry (IMS-MS) techniques. Mobility distributions of $[\text{L-Ser} + \text{M} + \text{H}]^+$ (where L-Ser is L-serine and M is a given monosaccharide), $[\text{L-Phe-Gly} + \text{M} + \text{H}]^+$ (where L-Phe-Gly is L-phenylalanine−glycine), and $[\text{Mn}^{\text{II}} + (\text{L-Phe-Gly} - \text{H}) + \text{M}]^+$ complex ions are used to determine collision cross sections (ccs in Å^2), and groups of cross sections for different clusters are proposed as means of identifying the sugar isomers. Within one type of complex, variations in ccs do not always allow delineation between the 16 glucose isomers, but interestingly, when ccs of three different ions are combined as a spatial vector, enantiomers are partially resolved. As a result of this analysis, L-glucose, D-glucose, L-allose, D-allose, D-gulose, D-galactose, and L-mannose are delineated, and for all eight enantiomeric pairs, D and L entities display different coordinates. In addition, different combinations of amino acids, peptide, and metal ions are surveyed, and the potential for yielding unique coordinates for the generated diastereomeric complexes is assessed.

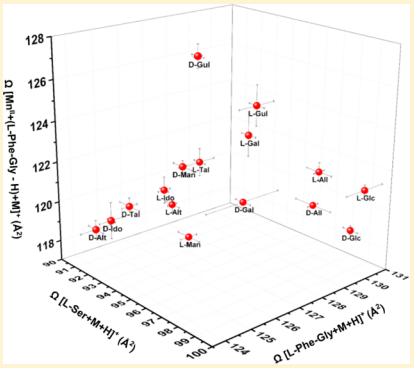

Because isomeric species, including not only diastereomers but also enantiomers, often differ in their physical properties[1,2] and biological activities,[3−6] their proper structural identification is key to the discovery of drugs and other bioactive compounds.[3,7] Enantiomeric pairs are currently characterized by high performance liquid chromatography (HPLC), capillary electrophoresis (CE), and nuclear magnetic resonance (NMR) spectroscopy.[3,7,8] Diastereomer identification methods routinely combine CE, HPLC, and other chromatographic techniques (e.g., gas chromatography, supercritical fluid chromatography) with mass spectrometry (MS), which has the advantages of high-throughput, of a low limit of detection, and of characterizing complex mixtures.[3,7] Mass spectrometry alone has even been used for chiral analysis using three main methodologies. In a first approach, one enantiomer is isotopically labeled to form transient diastereomeric adducts with a chiral selector, and as a result of a single-stage MS experiment, enantiomeric pairs are separated on the basis of their mass differences.[7,9] A second tactic is to allow enantiomers to react with a chiral selector. Isobaric diastereomeric complexes are generated and trapped in an MS instrument where a reaction occurs with a gas-phase reagent. In this methodology, separation of enantiomeric pairs is achieved by monitoring the rate at which enantiomers are displaced from the diastereomeric complex by the gas-phase reagent and by measuring the abundance of the newly formed adduct ion comprising the chiral selector and the gas-phase reagent.[7,9,10] The third type of chiral separation by MS alone is the kinetic method.[7,9,11−18] This method was first used to measure proton affinities of small molecules in the gas phase by dissociation of a proton-bound dimer.[11,12] Because the rates of fragmentations are proportional to the relative activation energies required to generate each proton bond monomer from the proton-bound dimer, a measurement of proton affinity of each monomer can be derived.[11,12] This procedure was applied to isomeric[17,18] and enantiomeric[13−16] distinction by competitively generating, with electrospray ionization[19] (ESI), a cluster ion made of the analyte, chiral selectors, and a divalent metal ion and by subsequently dissociating the diastereomeric complex formed by tandem MS (MS/MS). The kinetic method was then improved by replacing one of the chiral selectors by a fixed ligand (usually a chiral peptide strongly chelated to the analyte and unique site of deprotonation) in order to prevent ambiguous structural assignments.[20,21] Although the fixed ligand kinetic method was successfully used for the chiral characterization of amino acids,[21] chiral drugs,[20] and carbohydrates,[21−23] the use of MS/MS limits its high-throughput capabilities when not used in combination with condensed phase separation methods.

Recently, ion mobility spectrometry combined with mass spectrometry (IMS-MS) techniques have been developed for the analysis of diastereomers. In IMS-MS, ions are separated on the basis of their average collision cross section (ccs) resulting from collisions with a buffer gas, their charge (z) as they are transported through the buffer gas under the influence of an

Received: November 11, 2015
Accepted: January 22, 2016

DOI: 10.1021/acs.analchem.5b04280
Anal. Chem. XXXX, XXX, XXX−XXX

Scheme 1. Structures of the 16 Monosaccharides Characterized by IMS-MS[a]

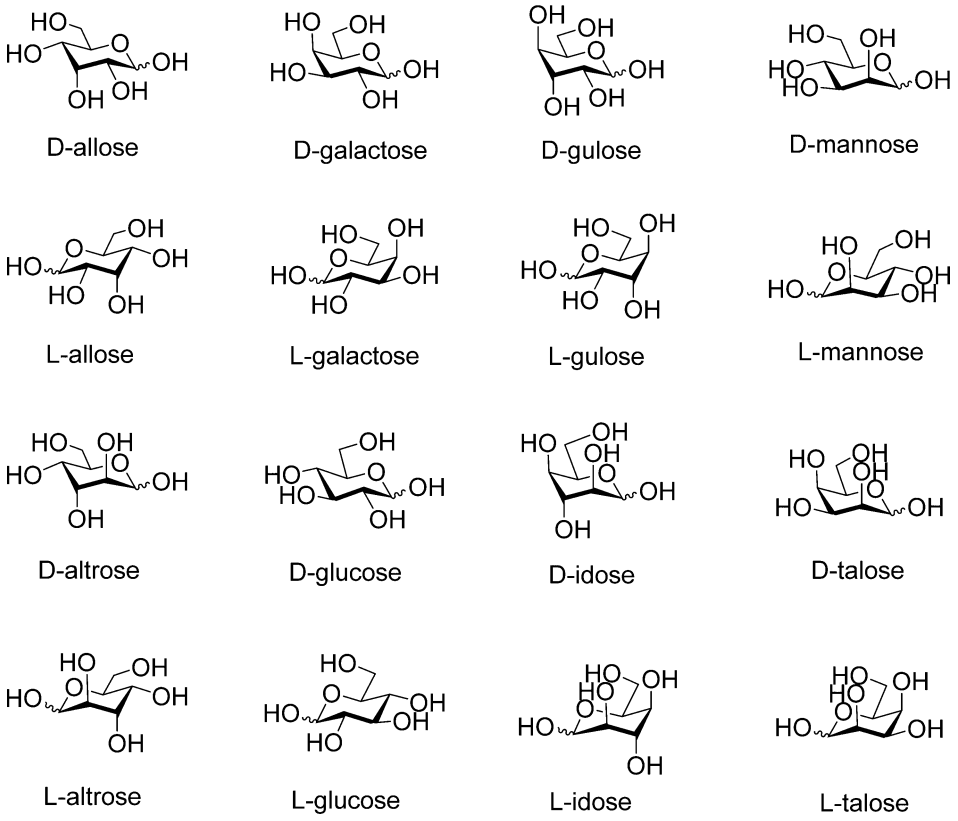

[a]Eight glucose diastereomers differing only by the number and position of axial hydroxyl groups on the pyranose ring, along with their respective enantiomers, are represented. Glucose (Glc), mannose (Man), altrose (Alt), idose (Ido), galactose (Gal), allose (All), talose (Tal) and Gulose (Gul).

electric field, and their mass.[24−26] To date, the inherent multidimensionality of a single IMS-MS experiment has been widely used for the separation of isomers[24−26] but to a lesser extent for chiral separation.[7] More recently, Campuzano and co-workers characterized two drug-like diastereomers as protonated ions with only 1 Å^2 difference in ccs (and a reported resolving power of 40) in nitrogen buffer gas.[27] In another study, Revesz and co-workers separated two protonated syn and anti enantiomers of a bis-Tröger base and improved the separation by forming sodiated species.[28] Likewise, Domalain and co-workers were able to distinguish a cis/trans pair of diastereomers by generating both monomers and dimers of analyte−alkali cation adducts.[29] Deprotonated ions of carbohydrates were also characterized recently with IMS-MS.[30] Field asymmetric IMS (FAIMS) was also used for chiral separation, and in 2008, Mie and co-workers reported the separation of drug compounds by forming diastereomeric complexes resembling the ones generated in the kinetic method.[31] The present work is also inspired by the fixed ligand kinetic method. Diastereomeric complexes comprising the analyte, a fixed ligand (single amino acid or peptide), and a divalent metal are generated by ESI and analyzed by IMS-MS. However, unlike the kinetic method experiment, these complexes are not dissociated, and enantiomers are directly characterized by the ccs in He buffer gas of diastereomeric complexes.

Recently, Nagy and Pohl[23] successfully developed a variant of the fixed ligand kinetic method to provide the first example of using mass spectrometry alone to differentiate all 16 isobaric glycopyranose isomers (Scheme 1), including the enantiomer pairs. Glucose has its hydroxyl groups on carbon 2 (C2), C3, and C4 of the pyranose ring all oriented equatorially. Shifting the orientation of one (as in allose, galactose, and mannose), two (as in altrose, gulose, and talose), or all three (as in idose) hydroxyl groups from equatorial to axial gives rise to seven additional isomeric species. In addition, each one of the eight regioisomers exists as a D or L enantiomer resulting in a total of 16 unique monosaccharides. Clearly, on the basis of this initial work, the energetic differences in dissociation of the carbohydrate analytes versus the ligands to metal-containing complexes could be diagnostic.[23] This discovery raised the interesting question as to whether the carbohydrate complexes themselves could be differentiated directly by their shape. With this in mind, dimeric and trimeric adduct ions, comprising a single enantiomer, are generated by ESI and analyzed by IMS-MS for each one of the 16 glucose isomers. Collision cross sections for selected complexes are derived and are combined into a multidimensional data set. As a result, each monosaccharide is characterized by a spatial vector, where each coordinate (x, y, z) is the ccs value (in Å^2) of a given complex ion. In addition, $[Co^{II} + (L\text{-aa} - H) + M]^+$ and $[Mn^{II} + (L\text{-aa} - H) + M]^+$ complexes (where L-aa is L-Ser (L-serine) or L-Asn (L-asparagine)) are investigated for D-altrose, D-idose, L-idose, and D-talose. Finally, the potential held by different peptides to distinguish D- and L-idose is evaluated by probing diastereomeric adducts formed with L-Pro-Gly (L-proline−glycine), L-Trp-Gly (L-tryptophan−glycine), and L-Tyr-Gly (L-tyrosine−glycine), respectively.

DOI: 10.1021/acs.analchem.5b04280
Anal. Chem. XXXX, XXX, XXX−XXX

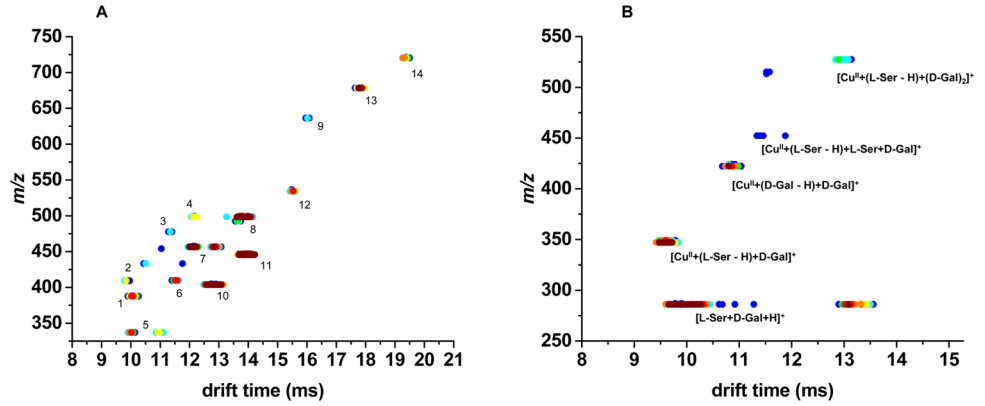

Figure 1. Nested t_D (m/z) two-dimensional spectra obtained from a solution of D-galactose with (A) L-Phe-Gly, L-Asp, and Mn(II) and with (B) L-Ser and Cu(II). In both spectra, ion intensities are on a color scale, red representing ions with higher intensity. Ions in spectrum (A) are numerically labeled, and the corresponding species are reported in Table 1. The features in spectrum (B) are indicated as an inset. Similar spectra were obtained for allose, altrose, glucose, gulose, idose, mannose, and talose enantiomeric pairs.

Table 1. Species Observed in the IMS-MS Analysis of a Mixture of D-Galactose, L-Phe-Gly, L-Asp, and Mn(II)

ion label[a]	monoisotopic mass	observed species
1	387.7	$[\text{L-Asp} + \text{L-Phe-Gly} + (\text{D-Gal})_2 + 2H_2O + Na + H]^{2+}$
2	408.6	$[Mn^{II} + \text{L-Phe-Gly} + (\text{D-Gal})_3]^{2+}$
3	477.7	$[\text{L-Asp} + \text{L-Phe-Gly} + (\text{D-Gal})_3 + 2H_2O + Na + H]^{2+}$
4	498.6	$[Mn^{II} + \text{L-Phe-Gly} + (\text{D-Gal})_4]^{2+}$
5	336	$[Mn^{II} + (X_1^{\text{L-Phe-Gly}} - H) + \text{D-Gal}]^+$
6	409	$[Mn^{II} + (\text{L-Phe-Gly} - H) + \text{L-Asp}]^+$
7	**456.1**	$[\mathbf{Mn^{II} + (L\text{-}Phe\text{-}Gly - H) + D\text{-}Gal}]^+$
8	498.1	$[Mn^{II} + (\text{L-Phe-Gly} - H) + \text{L-Phe-Gly}]^+$
9	636.1	$[Mn^{II} + (\text{L-Phe-Gly} - H) + (\text{D-Gal})_2]^+$
10	**403.2**	$[\mathbf{L\text{-}Phe\text{-}Gly + D\text{-}Gal + H}]^+$
11	445.2	$[(\text{L-Phe-Gly})_2 + H]^+$
12	534.1	$[Mn^{II} + (a_1^{\text{L-Phe-Gly}} - H) + (\text{D-Gal})_2]^+$
13	678.1	$[Mn^{II} + (\text{L-Phe-Gly} - H) + \text{L-Phe-Gly} + \text{D-Gal}]^+$
14	720.2	$[Mn^{II} + (\text{L-Phe-Gly})_2 + (\text{L-Phe-Gly} - H)]^+$

[a]Ion labels correspond to peaks labeled on the nested $t_D(m/z)$ spectrum in Figure 1A. Species indicated in bold are further analyzed in the Results and Discussion section, and their respective collision cross section values for the 16 glucose isomers are reported in Table S-1.

EXPERIMENTAL SECTION

Materials and Sample Preparation. Enantiomeric pairs of glucose, mannose, altrose, idose, galactose, allose, talose, and gulose (98% purity) were obtained from Carbosynth Ltd. (San Diego, LA) and used without derivatization. Monosaccharide structures are depicted in Scheme 1. L-Asp (L-aspartic acid; ≥99% purity), L-Ser (≥99% purity), L-Asn (≥99% purity), L-Phe-Gly (L-phenylalanine−glycine; ≥98% purity), L-Pro-Gly, manganese(II) chloride, copper(II) chloride, and cobalt(II) acetate were purchased from Sigma-Aldrich (St. Louis, MO). Dipeptides, L-Trp-Gly (≥95% purity) and L-Tyr-Gly (≥90% purity) were obtained from Anaspec (Fremont, CA). Solutions in water−methanol (1:1) are prepared: (1) monosaccharide (0.03 M), dipeptide (0.0125 M), single amino acid (0.0125 M), and divalent metal ion (5 mM) and (2) monosaccharide (0.02 M), single amino acid (0.02 M), and divalent metal ion (5 mM). All solutions are analyzed individually.

IMS-MS Measurements. Sixteen glucose isomers (Scheme 1) in solution with different combinations of amino acid, peptide, and divalent metal ion are analyzed using a home-built IMS-time-of-flight (TOF) MS instrument. The instrument as well as theoretical and experimental aspects of an IMS-MS measurement were previously reported[24−26,32−37] and are further described in the Supporting Information. Collision cross sections for the singly charged protonated dimeric complexes $[\text{L-Ser} + M + H]^+$ $(m/z$ 286) and $[\text{L-Phe-Gly} + M + H]^+$ $(m/z$ 403) and for the singly charged deprotonated trimeric complex $[Mn^{II} + (\text{L-Phe-Gly} - H) + M]^+$ $(m/z$ 456) are reported in Table S-1. The analyte ion complexes examined in further detail in the present work are chosen according to their ability to place glucose isomers at different locations on the three-dimensional representation of the data set and by using a screening approach based on previous analytes studied by Cooks and co-workers.[13−16]

RESULTS AND DISCUSSION

IMS-MS of a Mixture of D-Galactose, L-Phe-Gly, L-Asp, and Mn(II). Diastereomeric complexes are generated by ESI of solutions comprising an enantiomerically pure monosaccharide, L-Phe-Gly, L-Asp, and Mn(II), subsequently mobility separated in a 2 M long drift tube filled with He buffer gas, and finally mass analyzed by a TOF mass detector. As a result of this IMS-MS experiment, a nested t_D (m/z) spectrum is obtained for the 16 glucose isomers depicted in Scheme 1. Figure 1A illustrates the 2D-plot obtained for D-galactose where features are numerically labeled and the corresponding ion assignments are presented in Table 1. One of the advantages of IMS-MS is that analytes, which would not have been readily detected on an

DOI: 10.1021/acs.analchem.5b04280
Anal. Chem. XXXX, XXX, XXX−XXX

ESI mass spectrum, are now seen on the 2D-plot (e.g., complex ion 9, Figures 1A and S-1). Doubly charged complexes along with singly charged complexes with or without the sugar moiety are observed. Doubly charged species fall into two categories: $[\text{L-Asp} + \text{L-Phe-Gly} + (\text{D-Gal})_n + 2H_2O + Na + H]^{2+}$ with $n = 2$ or 3 (where Gal is galactose; features 1 and 3 in Figure 1A) and $[\text{L-Asp} + \text{L-Phe-Gly} + (\text{D-Gal})_n]^{2+}$ with $n = 3$ or 4 (features 2 and 4 in Figure 1A). When the sugar moiety is not present, different combinations are observed: an adduct of two L-Phe-Gly (feature 11, Figure 1A); Mn(II) with a deprotonated L-Phe-Gly and L-Asp (feature 6, Figure 1A); Mn(II) with one deprotonated L-Phe-Gly and one or two L-Phe-Gly (features 8 and 14, respectively, Figure 1A). The dimeric complex [L-Phe-Gly + D-Gal + H]$^+$ displays a single feature centered at $t_D \sim$ 12.8 ms (feature 10, Figure 1A). Interestingly, the same complex with the addition of Mn(II), [Mn^{II} + (L-Phe-Gly − H) + D-Gal]$^+$ (feature 7 Figure 1A), displays a more compact major conformation centered at $t_D \sim$ 12 ms and a minor conformation centered at $t_D \sim$ 12.8 ms. Two structurally related complexes with, in one case, an additional monosaccharide [Mn^{II} + (L-Phe-Gly − H)+$(\text{D-Gal})_2$]$^+$ (feature 9, Figure 1A) and, in another case, an additional L-Phe-Gly [Mn^{II} + (L-Phe-Gly − H) + L-Phe-Gly + D-Gal]$^+$ (feature 13, Figure 1A) are also observed. Features labeled 5 and 12 (Figure 1A) correspond to ions with a fragment of L-Phe-Gly and are due to impurities in the peptide analyte (Figure S-2). Diastereomeric complex ions [L-Phe-Gly + M + H]$^+$ (m/z 403) and [Mn^{II} + (L-Phe-Gly − H) + M]$^+$ (m/z 456), where M is a given glucose isomer, are further investigated.

IMS-MS of a Mixture of D-Galactose, L-Ser, and Cu(II). The t_D (m/z) spectrum obtained when a solution of D-galactose, L-Ser, and Cu(II) is analyzed by IMS-MS is depicted in Figure 1B. Similar 2D-plots are obtained for the remaining 15 glucose isomers shown in Scheme 1. Diastereomeric complex ions are observed from 286 m/z to 527 m/z and all species are singly charged. The most elongated structure is the [L-Ser + D-Gal + H]$^+$ ion (286 m/z, $t_D \sim$ 10 ms, Figure 1B). This structure is further studied in the present paper. As seen in the case of Mn(II) (features 10 and 7, Figure 1A) and illustrated here by the complex ion [Cu^{II} + (L-Ser − H) + D-Gal]$^+$ (347 m/z, $t_D \sim$ 9.5 ms, Figure 1B), upon binding of a divalent metal ion, more compact structures are generated. Three other complexes comprising a Cu(II) ion are depicted: [Cu^{II} + (L-Ser − H) + D-Gal]$^+$ with either an additional L-Ser (m/z 452) or an additional D-Gal (m/z 527). Finally, a complex comprising D-Gal and Cu(II) only is shown at m/z 422 and $t_D \sim$ 10.7 ms.

Mobility Distributions of Diastereomeric Complex Ions. Mobility distributions are derived from the nested t_D (m/z) measurement by integrating all m/z bins centered on the ion of interest, across a narrow range of m/z values, for each drift time bin. Figures S-3, 2, and S-4 portray mobility distributions for the diastereomeric complex ions of the 16 glucose isomers [L-Phe-Gly + M + H]$^+$ (m/z 403, Figure S-3), [Mn^{II} + (L-Phe-Gly − H) + M]$^+$ (m/z 456, Figure 2), and [L-Ser + D-Gal + H]$^+$ ion (286 m/z, Figure S-4), respectively. The average ccs of each species obtained from triplicate measurements is shown in Table S-1.

Collision cross sections for the [L-Phe-Gly + M + H]$^+$ diastereomeric complex with D-enantiomers (Figure S-3, top panels) range from 122.9 ± 0.6 Å^2 (D-altrose) to 129.7 ± 0.1 Å^2 (D-glucose). Altrose (Alt) is a glycopyranose isomer with two consecutive axial hydroxyl (OH) groups in positions C2 and C3, whereas all OH groups in glucose are oriented equatorially. This suggests that the interaction between L-Phe-Gly and a glycopyranose varies, not surprisingly, with respect to the orientation of OH groups, thus providing a way to delineate between isomers. Indeed, on the basis of protein−carbohydrate interaction studies and computational modeling, the interaction between a sugar moiety and the peptide backbone is believed to be mostly due to hydrogen bonding between the carbohydrate OH groups and both (or either) the *C*-terminal carbonyl (hydrogen bond donor) and the *N*-terminal amide (hydrogen bond acceptor) of the peptide moiety.[38−41] In addition, it is possible that peptides with a hydrophobic side chain establish van der Waals interactions with C6 of the glycopyranose.[40] The mobility distributions depicted in Figure S-3 suggest the existence of a correlation between the number of axial OH groups and the average ccs of the D-enantiomers when forming a complex with L-Phe-Gly: D-altrose (122.9 ± 0.6 Å^2, axial OH

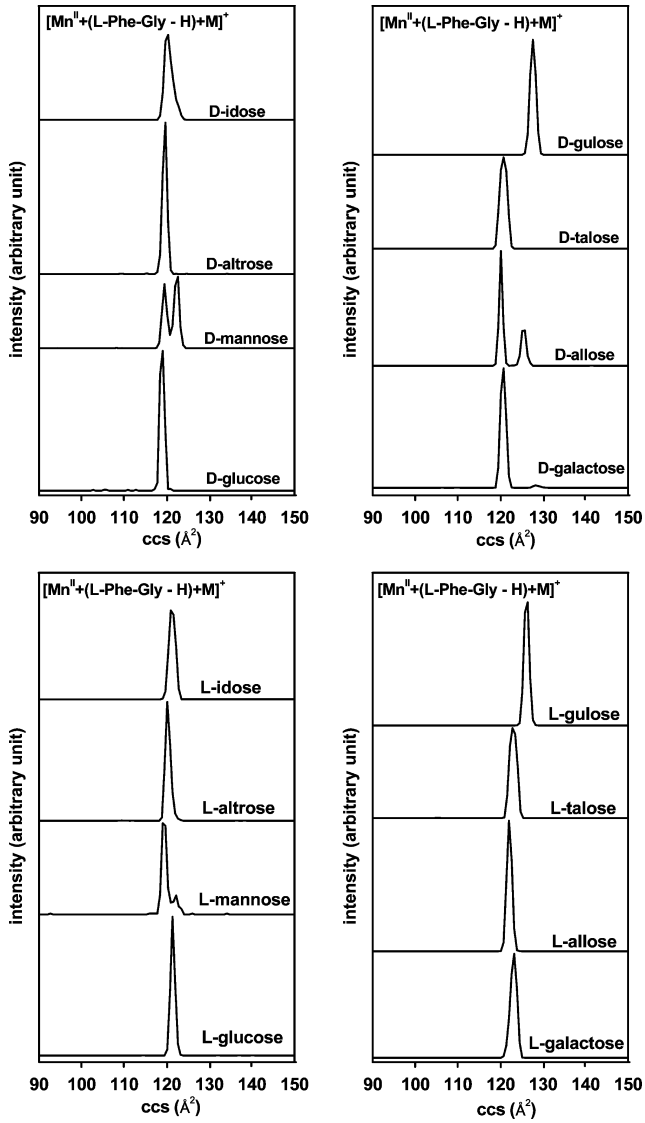

Figure 2. Mobility distributions of the singly charged deprotonated trimeric complex [Mn^{II} + (L-Phe-Gly − H) + M]$^+$ (m/z 456), where M is a given monosaccharide, for the eight diastereomers (D-enantiomers: top panels; L-enantiomers: bottom panels) represented in Scheme 1. The monosaccharide unit of the trimeric complex is indicated as an inset, and ccs (in Å^2) corresponding to the main feature of each mobility profile are reported in Table S-1.

DOI: 10.1021/acs.analchem.5b04280
Anal. Chem. XXXX, XXX, XXX−XXX

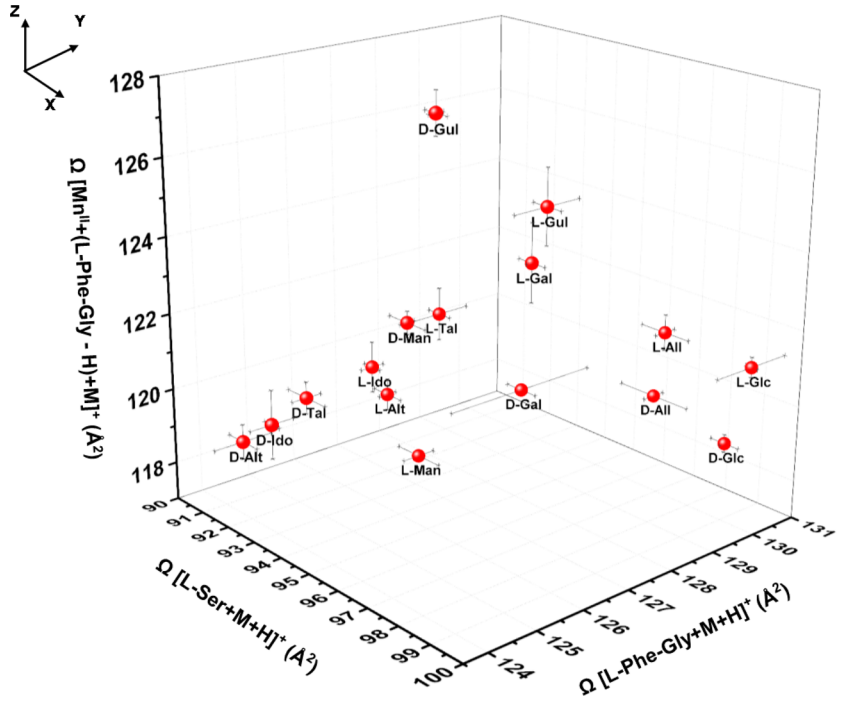

Figure 3. Three-dimensional representation of the collision cross sections (Ω in Å^2) of the singly charged protonated dimeric complexes [L-Ser + M + H]$^+$ (m/z 286, X-axis) and [L-Phe-Gly + M + H]$^+$ (m/z 403, Y-axis) and of the singly charged deprotonated trimeric complex [Mn^{II} + (L-Phe-Gly − H) + M]$^+$ (m/z 456, Z-axis) for the 16 monosaccharides depicted in Scheme 1. Error bars corresponding to standard deviations in all three dimensions are displayed.

at C2 and C3) ∼ D-idose (123.0 ± 0.4 Å^2, axial OH at C2, C3, and C4) < D-talose (124.1 ± 0.3 Å^2, axial OH at C2 and C4) < D-gulose (125.4 ± 0.2 Å^2, axial OH at C3 and C4) = D-mannose (125.4 ± 0.2 Å^2, axial OH at C2) < D-galactose (127.3 ± 1.5 Å^2, axial OH at C4) < D-allose (129.5 ± 0.2 Å^2, axial OH at C3) < D-glucose (129.7 ± 0.1 Å^2, no axial OH). That is, more compact structures are observed with a greater number of axial OH groups. The trend observed for complex ions formed with L-monosaccharides (Figure S-3, bottom panels) is similar (within experimental error), with the exception of the diastereomeric complex formed with L-mannose, which has a more compact structure than the one formed with L-talose and L-gulose, respectively. Overall, L-Phe-Gly interacts with the 16 glucose isomers giving rise to diastereomeric complexes within favorable characteristic ccs.

Trimeric complexes comprising Mn(II), deprotonated L-Phe-Gly, and a monosaccharide are observed for all 16 glucose isomers and depicted in Figure 2. To our knowledge, there is no known structure of such a complex. However, infrared multiple photon dissociation spectroscopy studies, in combination with quantum mechanical calculations, have shown that the lowest energy structure for a complex comprising a multiply charged transition metal and an amino acid is a charge-solvated tridentate complex with a deprotonated carboxylic acid terminus.[42] In addition, it has been demonstrated that metal ions form triply coordinated complexes with carbohydrates via three OH groups.[43−45] With this in mind, we can infer that both the monosaccharide and the peptide are bonded to the divalent metal ion, which is at the center of the trimeric complex [Metal^{II} + (L-peptide − H) + M]$^+$ characterized here. Mobility distributions for the diastereomeric complex [Mn^{II} + (L-Phe-Gly − H) + M]$^+$ with D-enantiomers are displayed in the top panel. Unlike the example of the complex without the divalent metal (Figure S-3), multiple features can be observed for D-allose, D-galactose, and D-mannose (Figure 2, top panel). Only ccs information for the main features are reported in Table S-1 and used in the following multidimensional analysis of diastereomers. It is interesting to note that the existence of multiple features allows further delineation between isomers as in the case of D-allose (major feature at 120.0 Å^2, minor feature at 125.8 Å^2) and D-galactose (major feature at 120.6 Å^2 and minor feature at 128.3 Å^2). In future studies, minor features could be used to weight the ccs value obtained for the main feature. The correlation between the number of axial OH and ccs observed earlier for the complex ion [L-Phe-Gly + M + H]$^+$ does not exist here, suggesting that the peptide does not interact directly with the monosaccharide in the case of the complex ion [Mn^{II} + (L-Phe-Gly − H) + M]$^+$. The carbohydrate moiety and the divalent metal ion most likely form a complex via hydrogen bonding with three OH groups on the glycopyranose. In addition, the deprotonated peptide and the divalent metal ion presumably establish three hydrogen bond type of interactions, and as a result, a trimeric complex comprising the dipeptide, carbohydrate, and metal ion in the center is formed. This putative structure is also supported by the observation of a more compact structure for the complex ion [Mn^{II} + (L-Phe-Gly − H) + D-Gal]$^+$ (m/z 456.1, feature 7, 120.6 Å^2, Figure 1A) than for the complex ion [L-Phe-Gly + M + H]$^+$ (m/z 403.2, feature 10, 127.3 Å^2, Figure 1A). That is, the deprotonated peptide is wrapped around the metal ion which itself is bonded to the carbohydrate. The mobility distribution for [Mn^{II} + (L-Phe-Gly − H) + M]$^+$ with L-enantiomers is depicted in the bottom panel (Figure 2). Only the mobility distribution for L-mannose displays two features at 119.1 and 122.2 Å^2, respectively. Remarkably, the same features are present in the mobility distribution for D-mannose (Figure 2, top panel). However, mobility distributions for D- and L-mannose differ by the relative abundances of compact (119.1

DOI: 10.1021/acs.analchem.5b04280
Anal. Chem. XXXX, XXX, XXX−XXX

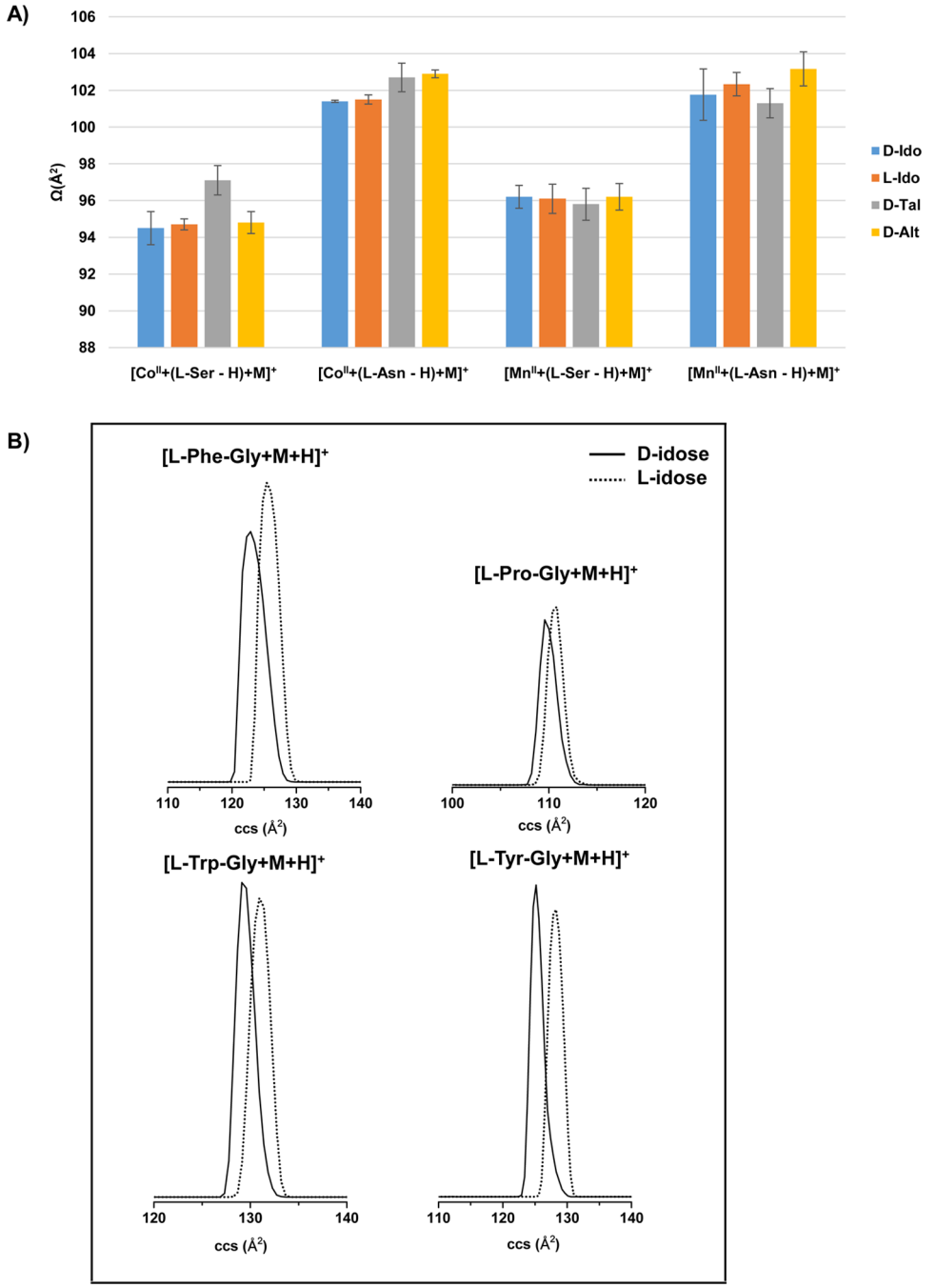

Figure 4. (A) Bar diagram of ccs (Ω in Å^2) obtained from triplicate measurements of the trimeric complex ions $[Co^{II} + (L\text{-Ser} - H) + M]^+$, $[Co^{II}+(L\text{-Asn} - H) + M]^+$, $[Mn^{II} + (L\text{-Ser} - H) + M]^+$, and $[Mn^{II} + (L\text{-Asn} - H) + M]^+$ for D-idose, D-talose, D-altrose, and L-idose. (B) Overlaid mobility distributions for D-idose (solid line) and L-idose (dashed line) in dimeric complex ions comprising the monosaccharide moiety and the dipeptides L-Phe-Gly, L-Pro-Gly, L-Trp-Gly, and L-Tyr-Gly, respectively.

Å^2) and elongated (122.2 Å^2) features, thus allowing distinction between the two enantiomers.

A variety of complex ions are characterized when D-galactose in solution with L-Ser and Cu(II) is analyzed by IMS-MS. We chose here to further study the dimeric complex ion $[L\text{-Ser} + M + H]^+$, and mobility distributions for D (top panel) and L (bottom panel) glucose isomers are depicted in Figure S-4. No obvious trend is observed in the ccs values. Complexes formed with D- and L-glucose are the most elongated structures (99.4 and 99.5 Å^2, respectively) as observed for the trimeric complex $[L\text{-Phe-Gly} + M + H]^+$. Within the D-monosaccharides (Figure S-4, top panel), D-mannose (95.3 Å^2), D-glucose, and D-allose (97.5 Å^2) are distinguishable only on the basis of the described ccs for the complex ion $[L\text{-Ser} + M + H]^+$. In the case of L-monosaccharides, unique ccs are reported for L-allose (97.9 Å^2) and L-glucose. In order to improve the delineation between the 16 glucose isomers depicted in Scheme 1, we propose here a multidimensional analysis of the ccs measured in He buffer gas for the complex ions $[L\text{-Ser} + M + H]^+$, $[L\text{-Phe-Gly} + M + H]^+$, and $[Mn^{II} + (L\text{-Phe-Gly} - H) + M]^+$.

Multidimensional Analysis of Diastereomers. Collision cross sections of the main feature in the mobility distributions

DOI: 10.1021/acs.analchem.5b04280
Anal. Chem. XXXX, XXX, XXX−XXX

of diastereomeric adducts [L-Ser + M + H]$^+$ (m/z 286), [L-Phe-Gly + M + H]$^+$ (m/z 403), and [Mn^{II} + (L-Phe-Gly − H) + M]$^+$ (m/z 456) (reported in Table S-1) are used as, respectively, x, y, and z coordinates in a three-dimensional (3D) representation of the data set. As a result, a 3D-plot comprising 16 points corresponding to the 16 monosaccharides depicted in Scheme 1 is obtained and shown in Figure 3. The standard deviation from independent triplicate measurements is used in all three dimensions as an indication of the experimental error on the ccs determination. In this newly created 3D analytical space, D-gulose, D-galactose, L-mannose, D- and L-allose, and D- and L-glucose are unambiguously distinguished from the other monosaccharides (Figure 3). The remaining enantiomers can be categorized into four different groups of monosaccharides and, within a group, enantiomers cannot be separated on the basis of the coordinates of the selected cluster ions. After a visual inspection of the 3D-plot shown in Figure 3, groups are defined as follows: (1) L-gulose and L-galactose, (2) D-mannose and L-talose, (3) L-idose and L-altrose, and (4) D-talose, D-idose, and D-altrose. Interestingly, for all 16 glucose isomers, it is possible to distinguish D- an L-enantiomers, although one enantiomer might not be distinguishable from another monosaccharide. For three enantiomeric pairs, each enantiomer belongs to a different group: L-talose (group 2) and D-talose (group 4); L-idose (group 3) and D-idose (group 4); L-altrose (group 3) and D-altrose (group 4). Lastly, for three enantiomeric pairs, one enantiomer belongs to one of the defined groups and the other is distinguishable from all other 15 monosaccharides; it is the case for L-gulose (group 1), L-galactose (group 1), and D-mannose (group 2). In addition to individual coordinates, the distribution of the different monosaccharides in the created 3D-space could provide additional information. For example, one can imagine a line going through D-galactose, D-allose, and D-glucose (Figure 3). Interestingly, a parallel line at higher ccs goes through L-galactose, L-allose, and L-glucose (in the same order along the X-axis). This suggests that the contribution of the complex ions [L-Ser + M + H]$^+$ and [L-Phe-Gly + M + H]$^+$ allowed individual discrimination of the three monosaccharides (galactose, allose and glucose) within an enantiomeric group (D or L), while the Z-axis ([Mn^{II} + (L-Phe-Gly − H) + M]$^+$) permitted the distinction between D and L enantiomeric pairs. Another example is the alignment of carbohydrates moieties along a line going from D-altrose to D-gulose (Figure 3). Taking into consideration the D-monosaccharides along this line shows that this distribution reflects the trend described earlier for the complex ion [Mn^{II} + (L-Phe-Gly − H) + M]$^+$ (Z-axis) establishing a correlation between the number of axial OH groups and ccs. On the basis of these observations, in the same way that chromatographic columns are combined in proteomics experiments, we can start to imagine combining different types of complex ions based on their ability to individually discriminate between isomers. Overall, although not all 16 glucose isomers are resolved on the basis of the reported ccs for the diastereomeric adducts [L-Ser + M + H]$^+$, [L-Phe-Gly + M + H]$^+$, and [Mn^{II} + (L-Phe-Gly − H) + M]$^+$, seven monosaccharides are unequivocally distinguished, and for all monosaccharides, D and L enantiomers have distinct coordinates. However, when enantiomers belong to one of the groups defined earlier, even though D and L enantiomers have different coordinates in the 3D-represention of the data set, an ambiguity remains with respect to the identity of the sugar (e.g., D- and L-talose are separated but D-talose can not be distinguished from D-altrose and D-idose within the experimental error). Because of this, diastereomeric complexes comprising monosaccharides belonging to group 1, along with L-idose, are further investigated with four combinations of amino acid and divalent metal ions. In addition, the enantiomeric pair D/L-idose is examined when associated with different peptides.

Evaluation of Different Combinations of Amino Acid, Peptide, and Metal Ions. A bar diagram of ccs obtained from triplicate measurements of the trimeric complex ions [Co^{II} + (L-Ser − H) + M]$^+$, [Co^{II}+(L-Asn − H) + M]$^+$, [Mn^{II}+(L-Ser − H) + M]$^+$, and [Mn^{II} + (L-Asn − H) + M]$^+$ for D-idose, D-talose, D-altrose, and L-idose is shown in Figure 4A, and associated ccs values are reported in Table S-2. The presence of Mn(II) and Co(II) divalent metal ions in complexes with L-Ser yields structures with ccs in the same order (∼94 to 97 Å^2). Interestingly, although the four monosaccharides are not distinguishable based on the [Mn^{II} + (L-Ser − H) + M]$^+$ complex ion, when bound to Co(II), D-talose, which was undistinguishable from D-idose and D-altrose in the initial analysis (Figure 3), displays now a unique ccs (97.1 Å^2, Figure 4A). The ability of carbohydrates to adopt different conformations when bound to a metal ion has been used previously for isomers delineation.[46−49] Likewise, [Co^{II}+(L-Asn − H) + D-Ido]$^+$ (where Ido is idose; 101.4 Å^2) and [Mn^{II} + (L-Asn − H) + D-Alt]$^+$ (103.2 Å^2) are delineated from the corresponding complex ions with D-talose and D-altrose and with D-idose and D-talose, respectively. In short, varying the amino acid or/and the metal ion in diastereomeric complexes led to different degrees of separation between glucose isomers.[31] However, the D/L-idose enantiomeric pair is not distinguishable in any of the above combinations (Figure 4A). Next, dimeric complexes comprising L-Phe-Gly, L-Pro-Gly, L-Trp-Gly, and L-Tyr-Gly are investigated for the distinction between D- and L-idose. Overlaid mobility distributions for D- and L-idose in the different complexes are displayed in Figure 4B (ccs are reported in Table S-3). For each one of the mobility profiles, the peak width and the full width at half-maximum (fwhm) are calculated. Peak-to-peak resolution ($R_{p\text{-}p}$) and resolving power (R_p) are next calculated on the basis of the equations used in liquid chromatography by substituting the retention time by the ccs.[50] The dipeptide L-Phe-Gly, initially used in the multidimensional analysis of the data set, yielded R_p values of 27.3 and 33.0 for [L-Phe-Gly + D-Ido + H]$^+$ and [L-Phe-Gly + L-Ido + H]$^+$, respectively, and a $R_{p\text{-}p}$ of 0.29. Although the $R_{p\text{-}p}$ for complexes comprising L-Pro-Gly is smaller (0.13), the R_p is greater for both D- and L-idose (53.0 and 57.0, respectively). Interestingly, both the R_p (55.6 for D-idose, 52.6 for L-idose) and the $R_{p\text{-}p}$ (0.35) are enhanced when L-Trp-Gly is used. A significant improvement in peak-to-peak resolution is observed for [L-Tyr-Gly + D-Ido + H]$^+$ and [L-Tyr-Gly + L-Ido + H]$^+$ (0.57). Because all four peptides are likely to establish hydrogen bonding with the monosaccharide OH groups via the C-terminal carbonyl and the N-terminal amide, differences in the reported $R_{p\text{-}p}$ are probably due to the nature of the peptide side chain. Indeed, as mentioned earlier, a monosaccharide moiety can establish van der Waals interactions with the hydrophobic side chain of a peptide.[40] In the present case, an increase in the $R_{p\text{-}p}$ is correlated to an increase in the side chain hydrophobicity.[51] Additionally, L-Tyr-Gly can establish an additional hydrogen bonding via the tyrosine side chain and thus yields a greater $R_{p\text{-}p}$.

DOI: 10.1021/acs.analchem.5b04280
Anal. Chem. XXXX, XXX, XXX−XXX

Additional combinations of amino acid, peptide, and metal ion are further examined. Collision cross sections of 10 different cluster ions for glucose isomers, which were not distinguished on the basis of the 3D-representation shown in Figure 3 (group 4, D-talose, D-idose, and D-altrose), are reported in Table S-4. L-Idose is also included in the analysis in order to assess the delineation between the two enantiomers D- and L-idose. Principal component analysis (PCA) is a multivariate analysis often used to reduce the dimensionality of a data set by finding directions of maximum variance within the data set.[52] The results of the PCA are represented in Figure S-5; the eigenvalues of the correlation matrix, as well as the extracted eigenvectors for the 10 cluster ions examined, are reported in Table S-5. In the present analysis, the two first principal components (PC1and PC2) account for 86.5% of the variance in the data set (Table S-5) and are represented in Figure S-5. Interestingly, all four glucose isomers are distinguished, including D- and L-idose enantiomers. D-Altrose and D-talose are mainly separated along the PC1 axis while the delineation between D-altrose, D-idose, and L-idose occurs along the PC2 axis. Individual contributions of each one of the 10 cluster ions to the observed differences in ccs are assessed by examining the coefficient of the extracted eigenvectors for the three first PC (Table S-5). A representation of the eigenvectors for PC1 and PC2 (loading plot) is overlaid on the representation of the two first PCs and shown in Figure S-5. Heavy loadings are observed along the PC1 axis for $[Mn^{II} + (L\text{-Ser-H}) + M]^+$, $[Mn^{II} + (L\text{-Pro-H}) + M]^+$, $[Co^{II} + (L\text{-Ser-H}) + M]^+$, and $[Co^{II} + (L\text{-Gln} - H) + M]^+$ (Figure S-5 and Table S-4). Complex ions contributing the most (in decreasing order) to the delineation between glucose isomers along PC2 are $[Mn^{II} + L\text{-Phe-Gly} - H + M]^+$, $[L\text{-Ser} + M + H]^+$, $[Co^{II} + (L\text{-Pro-H}) + L\text{-Pro} + M]^+$, and $[Co^{II} + (L\text{-Asn} - H) + M]^+$ (Figure S-5 and Table S-4). The use of PCA not only allows the examination of 10 ions simultaneously but also provides a tool for choosing combinations of amino acid, peptide, and metal ion for the delineation between isomers.

Increasing the Dimensionality of an IMS-MS Experiment by Combining Multiple Ion Collisional Cross Sections. Resolving powers for the cluster ions described in Figure 3 range from 24.8 to 127.2 and are reported in Table S-6. Associated $R_{p\text{-}p}$ values range from 0.1 to 1.4. In other words, if the selected cluster ions were represented in a single dimension, limited separation between isomers would be obtained. The peak capacity (n) is used as an estimation of the number of resolvable peaks in the 3D-space created by combining ccs for three cluster ions (Figure 3). Here, we define the peak capacity as the range over which peaks are separated divided by the average full width at half-maximum of selected ions.[53,54] In the spectra shown in Figure 1A,B, cluster ions are separated in a drift time range spanning from 9.78 to 19.5 ms and from 9.42 to 13.41 ms, respectively. The peak capacity of the created 3D analytical space (Figure 3) is obtained by multiplying the peak capacity associated with $[L\text{-Ser} + M + H]^+$ (n = 16) ion by the sum of peak capacities associated with $[L\text{-Phe-Gly} + M + H]^+$ and $[Mn^{II} + (L\text{-Phe-Gly} - H) + M]^+$ (n = 36 + 65). As the result, an overall peak capacity of 1616 is reported. That is, the combination of selected ions in a novel 3D-plot results in a significant gain in peak capacity. In theory, this space could be extended to as many dimensions (number of cluster ions) needed to obtain a complete separation of the data set.

CONCLUSION

Herein, ion mobility spectrometry was used to develop a new method to discriminate glycopyranose isomers based on the shapes of their respective chiral noncovalent complexes, as represented by their ccs values. These noncovalent complexes are formed via ESI of solutions containing a mixture of an enantiomerically pure monosaccharide, divalent metal cation, and an amino acid and/or peptide. Carbohydrate−peptide complexes are the result of interactions between OH groups on the glycopyranose and the peptide via its *C*-terminal carbonyl, *N*-terminal amide, and side chain. Likewise, a metal ion commonly interacts with a carbohydrate moiety via three OH groups of the glycopyranose. For diastereomeric complexes with a monosaccharide, a divalent metal ion, and a peptide (or a single amino acid), we infer that the metal ion is at the center of the complex and establish two tridentate interactions with the glycopyranose and the peptide, respectively. Because, from one glycopyranose isomer to another, the orientation of the OH groups changes, we report here the use of ccs of diastereomeric complexes in order to delineate between isomers. $[L\text{-Ser} + M + H]^+$, $[L\text{-Phe-Gly} + M + H]^+$, and $[Mn^{II} + (L\text{-Phe-Gly} - H) + M]^+$ ions are used as x, y, and z coordinates in a multidimensional representation of the data set. As a result of this analysis, D-gulose, D-galactose, L-mannose, D-allose, L-allose, D-glucose, and L-glucose are unambiguously distinguished from the other monosaccharides. For all enantiomeric pairs, D- and L-species have distinct coordinates. However, this analysis is limited by the existence of groups in which monosaccharide moieties are not resolved within experimental error. Such a group is D-altrose, D-idose, and D-talose (group 1). The ambiguity between these three glycopyranose isomers is resolved by using different combinations of divalent metal ion and amino acid. Indeed, $[Co^{II} + (L\text{-Ser} - H) + D\text{-Tal}]^+$, (where Tal is talose; 97.1 Å^2), $[Co^{II} + (L\text{-Asn} - H) + D\text{-Ido}]^+$ (101.4 Å^2), and $[Mn^{II} + (L\text{-Asn} - H) + D\text{-Alt}]^+$ (103.2 Å^2) display unique ccs when compared to the same complexes with the other two carbohydrates within group 1. Lastly, the contribution of the nature of the peptide in the figure of merits for the delineation between D- and L-idose is examined. We found that, among the tested peptides, L-Tyr-Gly yielded the best $R_{p\text{-}p}$ (0.57). This is most likely due to both van der Waals and hydrogen bond interactions between the monosaccharide and the tyrosine side chain. Although no complete individual discrimination of the glycopyranose isomers is obtained with the initial set of selected ions, the variety of complexes that are potentially formed upon ESI makes this methodology promising for the characterization of isomeric species. Because the concentration of peptide and monosaccharide analytes needed to yield complex ions of sufficient intensity is higher (mM range) than what is currently used for peptide and protein analysis using IMS-MS (μM range and lower concentrations), the following studies should attempt to improve the sensitivity of the proposed method. Such methodology might also include the use of PCA, as it allows the simultaneous examination of multiple complex ions. A better understanding of the interactions taking place within a diastereomeric complex ion, via computational modeling, for example, could be used to design specific metal/peptide probes for enantiomeric and diastereomeric delineation. Lastly, the combinations of multiple ions in a novel n-dimensional space, with each dimension represented by a given cluster ion ccs, show a potential in increasing the peak capacity of an IMS-MS

DOI: 10.1021/acs.analchem.5b04280
Anal. Chem. XXXX, XXX, XXX−XXX

experiment. Overall, this multidimensional representation of an IMS-MS data set, that is, using simultaneously a combination of ccs to characterize a given structure, could potentially be applied to oligosaccharides and other groups of chiral molecules.

From this study, along with previous work,[22,23] it has been shown that monosaccharides can be discriminated on the basis of unique chiral noncovalent complexes either through their shape/ccs (with ion mobility spectrometry) or their fragmentation pathways (through a variant of the kinetic method with tandem mass spectrometry). It is envisioned that these methods will be elegant complements to one another toward *de novo* carbohydrate sequencing.

■ ASSOCIATED CONTENT

Supporting Information

The Supporting Information is available free of charge on the ACS Publications website at DOI: 10.1021/acs.analchem.5b04280.

Experimental section; supplementary tables and figures. (PDF)

■ AUTHOR INFORMATION

Corresponding Author

*E-mail: mgaye@indiana.edu.

Notes

The authors declare no competing financial interest.

■ ACKNOWLEDGMENTS

This work is supported in part by the National Institutes of Health (NIH-5R01GM93322-2). We would also like to acknowledge the Joan and Marvin Carmack Chair funds for partial support of this work.

■ REFERENCES

(1) Perez-Garcia, L.; Amabilino, D. B. *Chem. Soc. Rev.* **2002**, *31*, 342−356.
(2) Myung, S.; Fioroni, M.; Julian, R. R.; Koeniger, S. L.; Baik, M.-H.; Clemmer, D. E. *J. Am. Chem. Soc.* **2006**, *128*, 10833−10839.
(3) Francotte, E.; Lindner, W., Eds. Chirality in Drug Research. In *Methods and Principles in Medicinal Chemistry*; Wiley: New York, 2006; Vol. 33.
(4) Jozwiak, K.; Plazinska, A.; Toll, L.; Jimenez, L.; Woo, A. Y. H.; Xiao, R. P.; Wainer, I. W. *Chirality* **2011**, *23*, E1−E6.
(5) Plazinska, A.; Kolinski, M.; Wainer, I. W.; Jozwiak, K. *J. Mol. Model.* **2013**, *19*, 4919−4930.
(6) Ciminiello, P.; Dell'Aversano, C.; Dello Iacovo, E.; Forino, M.; Tartaglione, L.; Pelin, M.; Sosa, S.; Tubaro, A.; Chaloin, O.; Poli, M.; Bignami, G. *J. Nat. Prod.* **2014**, *77*, 351−357.
(7) Awad, H.; El-Aneed, A. *Mass Spectrom. Rev.* **2013**, *32*, 466−483.
(8) Ward, T. J.; Baker, B. A. *Anal. Chem.* **2008**, *80*, 4363−4372.
(9) Schug, K. A.; Lindner, W. *J. Sep. Sci.* **2005**, *28*, 1932−1955.
(10) Speranza, M.; Gasparrini, F.; Botta, B.; Villani, C.; Subissati, D.; Fraschetti, C.; Subrizi, F. *Chirality* **2009**, *21*, 69−86.
(11) Shen, W. Y.; Wong, P. S. H.; Cooks, R. G. *Rapid Commun. Mass Spectrom.* **1997**, *11*, 71−74.
(12) Cooks, R. G.; Wong, P. S. H. *Acc. Chem. Res.* **1998**, *31*, 379−386.
(13) Augusti, D. V.; Carazza, F.; Augusti, R.; Tao, W. A.; Cooks, R. G. *Anal. Chem.* **2002**, *74*, 3458−3462.
(14) Tao, W. A.; Clark, R. L.; Cooks, R. G. *Anal. Chem.* **2002**, *74*, 3783−3789.
(15) Tao, W. A.; Zhang, D. X.; Nikolaev, E. N.; Cooks, R. G. *J. Am. Chem. Soc.* **2000**, *122*, 10598−10609.
(16) Tao, W. A.; Gozzo, F. C.; Cooks, R. G. *Anal. Chem.* **2001**, *73*, 1692−1698.
(17) Fouquet, T.; Charles, L. *J. Am. Soc. Mass Spectrom.* **2010**, *21*, 60−67.
(18) Major, M.; Fouquet, T.; Charles, L. *J. Am. Soc. Mass Spectrom.* **2011**, *22*, 1252−1259.
(19) Fenn, J. B.; Mann, M.; Meng, C. K.; Wong, S. F.; Whitehouse, C. M. *Mass Spectrom. Rev.* **1990**, *9*, 37−70.
(20) Wu, L. M.; Cooks, R. G. *Anal. Chem.* **2003**, *75*, 678−684.
(21) Wu, L.; Cooks, R. G. *Eur. Mass Spectrom.* **2005**, *11*, 231−242.
(22) Nagy, G.; Pohl, N. L. B. *Anal. Chem.* **2015**, *87*, 4566−4571.
(23) Nagy, G.; Pohl, N. L. B. *J. Am. Soc. Mass Spectrom.* **2015**, *26*, 677−685.
(24) Clemmer, D. E.; Jarrold, M. F. *J. Mass Spectrom.* **1997**, *32*, 577−592.
(25) Hoaglund, C. S.; Valentine, S. J.; Sporleder, C. R.; Reilly, J. P.; Clemmer, D. E. *Anal. Chem.* **1998**, *70*, 2236−2242.
(26) Collins, D. C.; Lee, M. L. *Anal. Bioanal. Chem.* **2002**, *372*, 66−73.
(27) Campuzano, I.; Bush, M. F.; Robinson, C. V.; Beaumont, C.; Richardson, K.; Kim, H.; Kim, H. I. *Anal. Chem.* **2012**, *84*, 1026−1033.
(28) Revesz, A.; Schroder, D.; Rokob, T. A.; Havlik, M.; Dolensky, B. *Angew. Chem., Int. Ed.* **2011**, *50*, 2401−2404.
(29) Domalain, V.; Tognetti, V.; Hubert-Roux, M.; Lange, C. M.; Joubert, L.; Baudoux, J.; Rouden, J.; Afonso, C. *J. Am. Soc. Mass Spectrom.* **2013**, *24*, 1437−1445.
(30) Hofmann, J.; Hahm, H. S.; Seeberger, P. H.; Pagel, K. *Nature* **2015**, *526*, 241−244.
(31) Mie, A.; Ray, A.; Axelsson, B. O.; Jornten-Karlsson, M.; Reimann, C. T. *Anal. Chem.* **2008**, *80*, 4133−4140.
(32) Koeniger, S. L.; Valentine, S. J.; Myung, S.; Plasencia, M.; Lee, Y. L.; Clemmer, D. E. *J. Proteome Research* **2005**, *4*, 25−35.
(33) Koeniger, S. L.; Merenbloom, S. I.; Valentine, S. J.; Jarrold, M. F.; Udseth, H.; Smith, R.; Clemmer, D. E. *Anal. Chem.* **2006**, *78*, 4161−4174.
(34) Merenbloom, S. I.; Koeniger, S. L.; Bohrer, B. C.; Valentine, S. J.; Clemmer, D. E. *Anal. Chem.* **2008**, *80*, 1918−1927.
(35) Shaffer, S. A.; Prior, D. C.; Anderson, G. A.; Udseth, H. R.; Smith, R. D. *Anal. Chem.* **1998**, *70*, 4111−4119.
(36) Tang, K.; Shvartsburg, A. A.; Lee, H.; Prior, D. C.; Buschbach, M. A.; Li, F.; Tolmachev, A.; Anderson, G. A.; Smith, R. D. *Anal. Chem.* **2005**, *77*, 3330−3339.
(37) Revercomb, H. E.; Mason, E. A. *Anal. Chem.* **1975**, *47*, 970−983.
(38) Bohrer, B. C.; Clemmer, D. E. *J. Am. Soc. Mass Spectrom.* **2011**, *22*, 1602−1609.
(39) Cocinero, E.J.; Carcabal, P.; Vaden, T. D.; Simons, J. P.; Davis, B. G. *Nature* **2011**, *469*, 76−80.
(40) May, A. P.; Robinson, R. C.; Vinson, M.; Crocker, P. R.; Jones, E. Y. *Mol. Cell* **1998**, *1*, 719−728.
(41) Guan, R. J.; Brown, P. H.; Swaminathan, C. P.; Roychowdhury, A.; Boons, G. J.; Mariuzza, R. A. *Protein Sci.* **2006**, *15*, 1199−1206.
(42) Hofstetter, T. E.; Howder, C.; Berden, G.; Oomens, J.; Armentrout, P. B. *J. Phys. Chem. B* **2011**, *115*, 12648−12661.
(43) Lalezari, P.; Jiang, A. F. *Vox Sang.* **1984**, *47*, 146−156.
(44) Gyurcsik, B.; Nagy, L. *Coord. Chem. Rev.* **2000**, *203*, 81−149.
(45) Fabian, W. M. F. *Theor. Chem. Acc.* **2007**, *117*, 223−229.
(46) Plasencia, M. D.; Isailovic, D.; Merenbloom, S. I.; Mechref, Y.; Clemmer, D. E. *J. Am. Soc. Mass Spectrom.* **2008**, *19*, 1706−1715.
(47) Yu, X.; Huang, Y. Q.; Lin, C.; Costello, C. E. *Anal. Chem.* **2012**, *84*, 7487−7494.
(48) Asam, M. R.; Glish, G. L. *J. Am. Soc. Mass Spectrom.* **1997**, *8*, 987−995.
(49) Huang, Y. T.; Dodds, E. D. *Anal. Chem.* **2013**, *85*, 9728−9735.
(50) Domalain, V.; Hubert-Roux, M.; Lange, C. M.; Baudoux, J.; Rouden, J.; Afonso, C. *J. Mass Spectrom.* **2014**, *49*, 423−427.
(51) Wimley, W. C.; Creamer, T. P.; White, S. H. *Biochemistry* **1996**, *35*, 5109−5124.

DOI: 10.1021/acs.analchem.5b04280
Anal. Chem. XXXX, XXX, XXX−XXX

(52) Jolliffee, I. T. *Principal Component Analysis*; Springer-Verlag: New York, 1986.
(53) Valentine, S. J.; Kulchania, M.; Srebalus Barnes, C. A.; Clemmer, D. E. *Int. J. Mass Spectrom.* **2001**, *212*, 97−109.
(54) Merenbloom, S. I.; Bohrer, B. C.; Koeniger, S. L.; Clemmer, D. E. *Anal. Chem.* **2007**, *79*, 515−522.

DOI: 10.1021/acs.analchem.5b04280
Anal. Chem. XXXX, XXX, XXX−XXX